16th World Congress in Computational Mechanics (WCCM)
21-26 July 2024, Vancouver, Canada
A. Korobenko, M. Laforest, S. Prudhomme, R. Vaziri (Eds)

# POSSIBILITIES FOR NUMERICAL MODEL VALIDATION THROUGH COMPUTED TOMOGRAPHY MEASURED DATA

**MATTHIAS PAHN[1], CHRISTOPH DE SOUSA[1], SZYMON GRZESIAK[1], FRANK LIEBOLD[2], JOSIANE GIESE[2], MANFRED CURBACH [2] AND BIRGIT BECKMANN[2]**

[1]RPTU University of Kaiserslautern-Landau
67663 Kaiserslautern, Germany
matthias.pahn@rptu.de and rptu.de/projekte/gulliver

[2]TUD Dresden University of Technology
01219 Dresden, Germany
birgit.beckmann@tu-dresden.de and massivbau.tu-dresden.de

**Key words:** Computed Tomography, Carbon-Reinforced Concrete, DVC, FEM

**Abstract.** In order to make accurate predictions of the structural behaviour of non-metallic reinforced concrete elements, one of the key problems in the development of this type of new material system is the capacity of modelling the load transfer mechanisms between the concrete matrix and the reinforcement elements. To predict the load-deflection response up to ultimate limit state conditions, a wide range of numerical simulation approaches, with capability of modelling the bond behaviour between the different materials has been proposed over the years and compared to experimental results. This research work presents new possibilities for comparing numerical finite elements models with laboratory data generated by computed tomography, namely in the context of three-point bending tests performed on carbon-reinforced concrete specimens. The aim is to present the potential of in situ computed tomography for validation of numerical simulations. Examples of computed tomography generated quantitative results and data visualisation are shown, which focus on generated displacement fields and crack patterns.

## 1 INTRODUCTION

Concrete is the world´s most produced material and the second-most consumed material globally after water [1]. In view of this, related research and development is of crucial importance worldwide, aiming for greater sustainability and for the urgent need to help mitigate climate change. One way to increase resource efficiency in concrete construction is through the use of non-metallic reinforcement solutions, such as carbon reinforcement, which enable the design of thinner load-bearing structures [2] and promote a reduction of concrete volume consumption. To exploit the sustainability potentials and ensure the safety as well as durability of structural members made of this composite material, it is crucial to understand its mechanical properties. The experimental characterization of the concrete's micro-structure including the analysis of damage mechanisms such as cracks are an ongoing subject of research in civil

engineering. Yet, investigations of crack formation under load are often restricted to the visual examination of the concrete's surface.

Computed tomography (CT) can be used to capture non-destructive cross-sectional images of concrete samples by exposing them to X-rays. When assembled, three-dimensional images are produced, providing information about the inner structure with the possibility of enabling full 3D characterization of internal damage such as cracks [3–5]. CT has hence become an increasingly relevant tool in the construction sector throughout the last decades, yielding studies that were previously unimaginable, as covered in recent literature reviews [6–8].

CT technology has also evolved to the point where X-ray scans can be performed while subjecting specimens to progressive loading conditions using in situ CT tests [9]. The resulting 4D datasets deliver holistic information about crack formation processes that are captured spatially (3D images) and temporally (for different load/time intervals). A number of papers have been published in recent times reporting investigations involving the emerging in situ CT approach, using different types of loading configurations on concrete samples, such as: uniaxial loading in compression [10,11] and tension [12], bending tests [13–15] splitting tests [5] and pull-out tests [9]. These research works have however been conducted using micro-CTs, which limits the maximum X-ray energy levels and sample size. Within the mentioned experiments, a maximum sample cross-section size of $75 \times 75$ mm$^2$ and a maximum X-ray scanning voltage of 210 keV were reported. The present study has unprecedented features in this regard, using energies of 8 MeV and a test setup that enables scanning specimens with cross-sections up to $80 \times 160$ mm$^2$.

Also in the case of numerical modelling, there has been a mounting interest on the use of CT-image-based finite element models to estimate the mechanical properties of concrete. CT is used in this case to accurately obtain the morphology of concrete's heterogeneous meso-structure, commonly characterised by aggregates, macro-pores and cement matrix. The segmented CT data, obtained through image processing algorithms, is then given as an input to a 3D meso-scale model [12,16–18]. Different material laws and approaches can then be applied to model the interfacial transition zone between elements such as aggregates [12,19,20] and fibres [15] and the surrounding matrix. The use of in situ CT allows furthermore for the validation of these models by providing a real 3D representation of the progression of damage and deformation due to external loading [11,19,21]. This is particularly important for the validation of cracking mechanisms on advanced numerical models cable of simulating a realistic 3D nonplanar crack propagation process [20]. The combination of CT scans and meso-scale modelling provides a comprehensive framework to understand the mechanical behaviour of composite materials on a microscopic level. However, images obtained through micro-CT technology are usually restricted to limited fields-of-view and small specimen dimensions and the extrapolation from mesoscale models to a macroscopic scale is yet to be thoroughly investigated.

This paper presents results of a preliminary in situ CT bending tests on carbon-reinforced concrete (CRC) beams that were conducted at the *Fraunhofer Development Centre X-ray Technology* (EZRT) in Fürth, Germany, using the X-ray detector that will be installed at *Gulliver* (see Section 2) and similar X-ray energy levels. The primary objective of these experiments was to visualize and analyse the development of load induced cracks on the CRC beams. To achieve this, the propagation of cracks was investigated at various load levels using CT during the bending tests. In this context, the present paper is the third part of an extended

research work conducted in the scope of the collaborative research centre/transregio TRR280 “Design strategies for material-minimized carbon reinforced concrete structures" [22]. The first two parts focused on the validation of CT data through comparison with other measurement techniques [23] and on the application of methods such as digital volume correlation and grayscale profile analysis for the determination of crack width [24]. This third part aims at providing a different perspective on the CT results, now focused on possible comparison procedures for FEM-based numerical simulations.

## 2 THE TOMOGRAPHY PORTAL “GULLIVER”

At the University of Kaiserslautern-Landau (RPTU), a worldwide unique tomography portal called “Gulliver” is currently on the last stages of development (see Figure 1a), which enables investigations on full-scale structural building components subjected to load increase while performing high-resolution computed tomography scans. The aim of this XXL-CT is to use computed tomography to deepen the understanding of the load bearing and deformation behaviour of concrete members under failure. Funded by the German Research Foundation (DFG), *Gulliver* is a central component of the Civil Engineering Technology Centre (BIG) at the RPTU in Kaiserslautern.

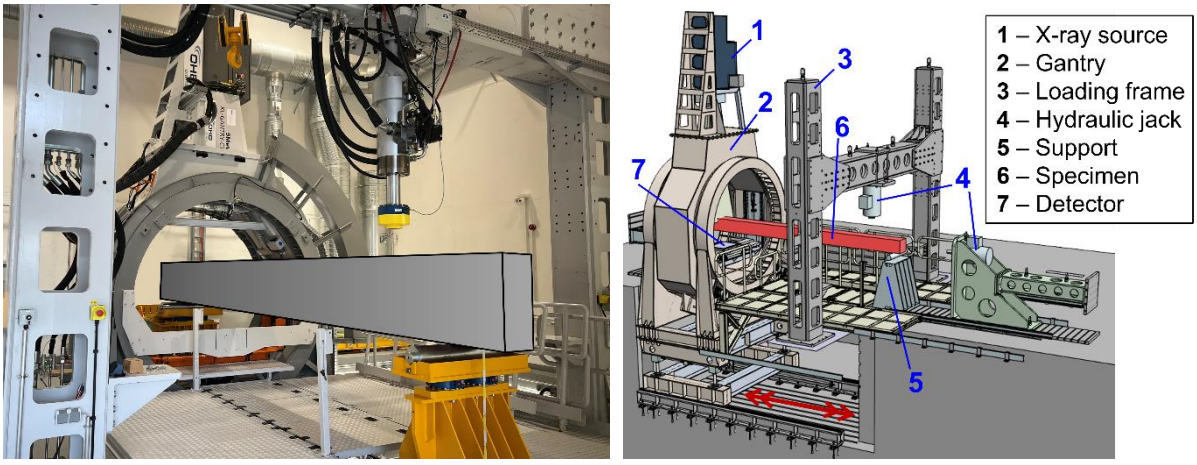


(a) (b)

**Figure 1**: The tomography portal “Gulliver” at the University of Kaiserslautern-Landau: (a) photo with artificial representation of the beam specimen; (b) identification of component parts

To enable high-quality image-based analysis of building components and structures under loading conditions, *Gulliver* is distinguished by its unique technical features (see Figure 1b). The built-in X-ray linear accelerator is mounted on a gantry that is able to rotate around the sample’s cross-section and move along the sample’s longitudinal axis. The linear accelerator provides X-ray energy of up to 9 MeV. The CT imaging system is equipped with three detectors of different characteristics, to enable dynamic measurements depending on the sample size and loading conditions: (i) X-ray detector *XEye* 5009 HE for scans on medium to large samples (field of view 500 × 90 mm$^2$, 10000 × 1900 pixels with pixel size 50 µm); (ii) X-ray flat panel detector *Varex* 4343 HE for scanning smaller test specimens (field of view 400 × 400 mm$^2$, 3072 × 3072 pixels with pixel size 139 µm); and (iii) high speed detector for fast scans during cyclic load application (field of view 300 × 150 mm$^2$, 1000 × 500 pixels with pixel size 300 µm

and maximum frame rate 300 Hz).

In terms of loading capabilities, *Gulliver*'s loading test bench enables both static (up to 600 kN in compression and 300 kN in tension) and dynamic loading (up to 300 kN in compression and 300 kN in tension) in the transverse and longitudinal direction of the specimen. The arrangement of supports can be customised and adjusted along the longitudinal direction of the sample. The maximum allowable dimensions for the test specimens are 6000 mm (length)× 1000 mm (max. width for 300 mm height) × 700 mm (max. height for 300 mm width).

The in situ CT tests reported in this paper were conducted using a radiation source similar to the one mentioned above, namely a linear accelerator (linac) with a current of 500 mA and energy of 8.0 MeV, and *Gulliver*'s the *Varex* detector. This means that each projection image had a resolution of 3072 × 3072 pixels, pixel size of 13 µm and a sensitive area of 400 × 400 $mm^2$. The test rig and the samples (see Section 3.1) were placed on a rotating platform in between the linac and the detector. The number of projections was limited by rotating the specimens by only 200°. Each scan took approximately 20 min for a total of 1300 projections.

## 3 IN SITU COMPUTED TOMOGRAPHY TESTS

### 3.1 Test setup, specimens and loading procedure

Figure 2a shows the test setup that was used during the in situ CT tests. The loading configuration consists on a three-point bending test performed on a pair of standing beam samples. The load was applied and measured using two hydraulic cylinders and two load cells positioned at the top and bottom ends of the beams. The test setup is complemented by a steel rod and two metal plates, which form the central support of the loading system (white objects visible in Figure 4b). This special loading configuration was developed specifically for the execution of in situ CT tests using a rotating table. The presence of two separate load application apparatuses on the beam ends, detached from each other, allow for a free measurement field during CT scans on the central portion of the samples (see yellow box in Figure 2b), where the highest level of damage is expected to occur. The measurement field was restricted to a 400 mm extension along the samples' longitudinal axis.

The specimen geometry is illustrated in Figure 2b. The CRC beams have a length of 600 mm and a cross-section of 80 × 80 $mm^2$. The adopted beam geometry also features a notch at the central cross-section with a depth of 3 mm (aligned with the steel rod support). The location of the carbon grid, placed at the tension zone of the specimens, is also shown in Figure 2b. The adopted carbon reinforcement consists of a grid with six warp threads in longitudinal direction. The adopted concrete cover thickness was equal to 5 mm.

The CT scans were performed on a total of four loading steps (see Table 1), with the aim of capturing the crack propagation process at different stages. The first CT scan was performed at load step 0, to capture the initial/unloaded state of the samples. Three additional scans were performed afterwards, for applied loads corresponding to 2 kN, 4 kN and 6 kN. The indicated load levels were kept constant during the scans.

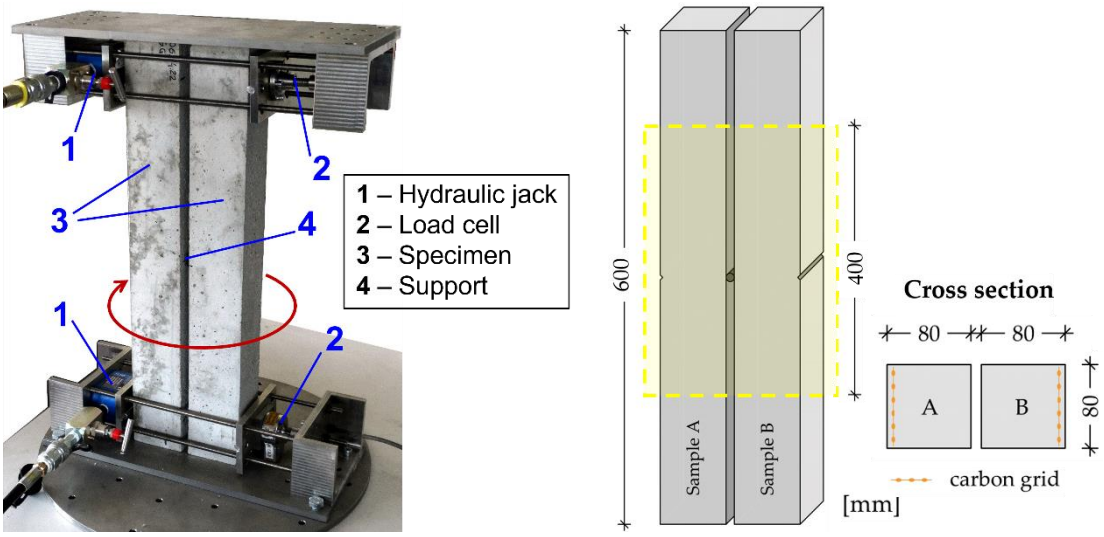


(a) (b)

**Figure 2**: Test setup and specimens: (a) three-point bending test setup; (b) specimen geometry

**Table 1**: Load steps for the in situ CT scans

| **Step** | 0 | 1 | 2 | 3 |
|---|---|---|---|---|
| **Load** | 0 kN | 2 kN | 4 kN | 6 kN |

## 3.2 Materials

The CRC samples investigated in this research work are composed by a fine-grained concrete matrix and a carbon fibre reinforced polymer textile reinforcement (see carbon grid in Figure 2b). The referred cementitious matrix consisted of a self-compacting and high-strength concrete, specifically designed for CRC structures. This concrete mixture composition, shown in Table 2, developed in the scope of the $C^3$ research project [25]. Due to the small size of the carbon grid, a maximum aggregate size of 2 mm was chosen. The binder concept adopted for this matrix was based on Portland cement, slag and limestone flour. In terms of material characterisation, the concrete matrix registered, at the day of testing, a compressive strength and bending tensile strength equal to 113.3 MPa and 12.5 MPa, respectively. The mean modulus of elasticity of this concrete was determined on a previous research work [26], where a mean value of 44 GPa was reported.

**Table 2**: Concrete mixture composition

| **Component** | Binder | Fine silica sand | Sand (2 mm) | Superplasticizer | Water |
|---|---|---|---|---|---|
| **Content [kg/m$^3$]** | 815 | 340 | 965 | 17 | 190 |

The planar textile reinforcement consists of a bidirectional warp-knitted grid made of carbon fibre yarns with a polyacrylate coating. This carbon grid is characterised by a reinforcement area in the longitudinal and transverse directions of 141 mm$^2$/m and 28 mm$^2$/m, respectively. Its material properties are defined by a tensile strength of 2200 MPa, a modulus of elasticity of 195 GPa and an ultimate strain equal to 11,3 ‰.

# 4 CT RESULTS FOR FEM VERIFICATION

## 4.1 3D deformation analysis

A popular subvoxel-accurate method for this is digital volume correlation (DVC) [27], which is an extension from digital image correlation (DIC) – from pixel to voxel data. Like DIC, DVC also requires a suitable texture in the CT image data. Deformation measurement and crack detection when using DVC is often performed by computing strains [28].

In this research work, the first step was the computation of a subvoxel-precise 3D displacement field by means of the method presented in [29]. This was applied to a regular grid of points with a spacing of 20 voxels where points with insufficient contrast in their neighbourhood were excluded. Subvolumes with dimensions of $25 \times 25 \times 25$ voxels surrounding the referred points were then used to calculate displacements.

Figure 3 shows a sequence of displacement vector fields between the reference state (load step 0) and the deformed states of load steps corresponding to load levels of 2 kN (Figure 3a), 4 kN (Figure 3b) and 6 kN (Figure 3c). It can be seen that the curvature induced in the beam samples due to bending loading led to higher levels of deformation on their upper half, with maximum shift (approximately 3 mm) being registered for the left beam (sample A).

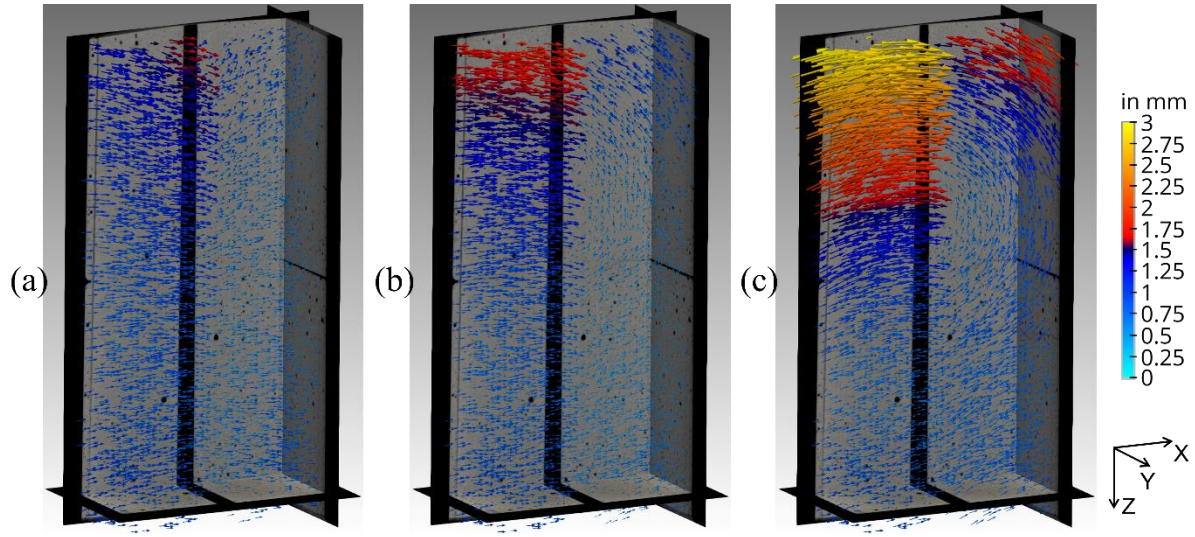


**Figure 3**: Generated displacement vector fields: (a) load step 1; (b) load step 2; (c) load step 3

## 4.2 3D crack width analysis

The crack measurement and analysis were done by applying the method of Liebold and Maas [30] with another deformation model being used, focused on profile analysis of the deformation field, for the automatic determination of crack widths. In the referred method, the points of the displacement field were triangulated in a tetrahedral mesh and each tetrahedron was analysed for changes between load steps. The model involved splitting the tetrahedron into two parts, with a relative translation between the parts where two cases were distinguished. This relative shift, $\vec{t}_{rel}$, was used as a deformation vector, and the norm of it, $|\vec{t}_{rel}|$, served as a scalar deformation that helped to identify tetrahedra containing a crack by applying a thresholding.

An illustration of the tetrahedral mesh distributed along the entirety of the tested samples is shown in Figure 4a. A reduced mesh is depicted in this case, for a more convenient visualisation. Figure 4b shows the adopted tetrahedral mesh superimposed with a 2D cut at the region of first crack formation.

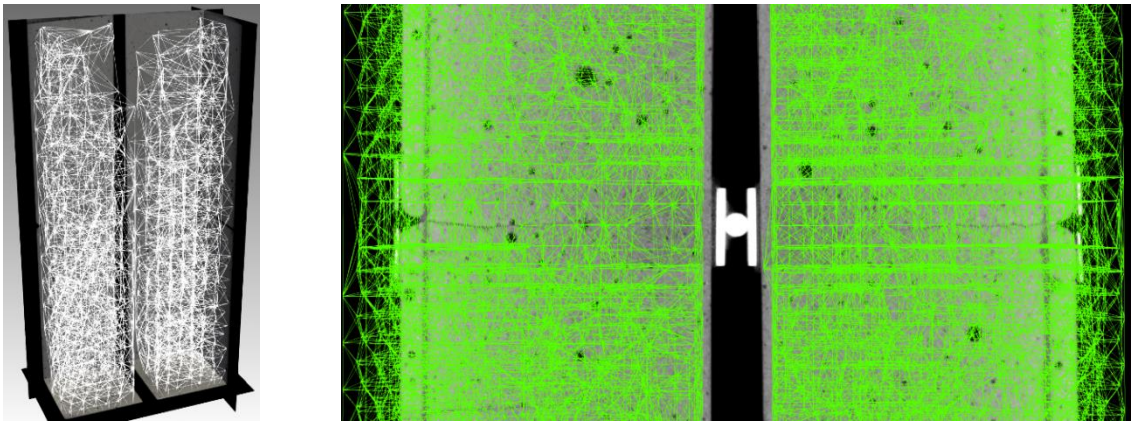

(a) (b)

Figure 4: Computed tetrahedral mesh: (a) 3D perspective (reduced mesh refinement); (b) close-up at region of crack formation (original mesh refinement)

In contrast to the method of [30], the automatic crack width detection in this research work was done by profile analysis of the deformation field ($|\vec{t}_{rel}|$), due to the high noise in the CT image data. At user-defined profiles, the crack width measurement was performed as follows: (i) detection of deformed tetrahedra along the profiles, where the scalar deformation exceeded a user-defined threshold for $|\vec{t}_{rel}|$; and (ii) inclusion of deformed neighbours of the previously identified tetrahedra, to compute a median vector of the deformation vectors. The norm of the median vector was used as the crack width. A more detailed description of this process can be found in [24].

Figure 5 shows the color-coded visualization of crack width results for the different load steps. It can be seen that no crack was detected at load step 1 (2 kN). First cracks were identified for the at 4 kN of load application (see Figure 5b) at notch location for both specimens. The obtained average crack width values for this load step (at carbon grid level) were equal to 0,21 m and 0,22 mm for samples A and B, respectively. At load step corresponding to 6 kN load application, several cracks were identified in the tension zone of the tested beams (four and three cracks in samples A and B, respectively). For this final load step, the average crack width at notch location was expectedly higher, reaching 0,26 mm and 0,31 mm for samples A and B, respectively. The obtained crack width values were subject to validation through direct comparison with other measurement techniques, as detailed in [23].

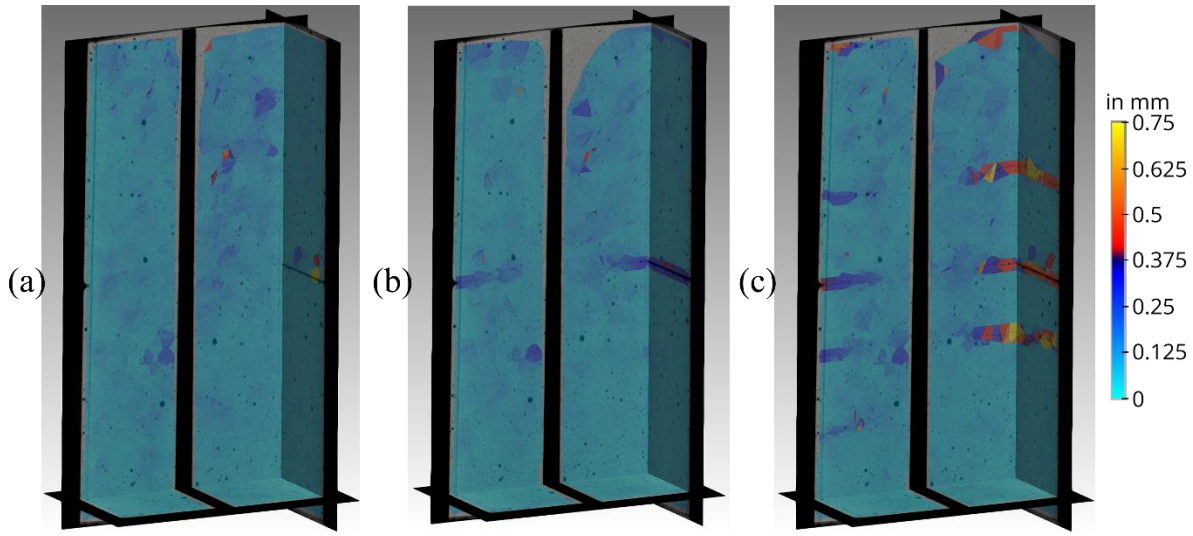


**Figure 5**: Internal cross-sections showing crack formation through color-coded visualization: (a) load step 1; (b) load step 2; (c) load step 3

### 4.3 Quality control procedures

The exact position of the reinforcement elements within the concrete matrix is traditionally determined by inspection and measuring of saw-cut planes or by using non-destructive tools such as electromagnetic concrete cover meters, which can determine the approximate location of steel reinforcement bars and a localized rough estimation of the concrete cover thickness. Through the obtained CT data, however, a truly precise and non-destructive 3D visualization and localization of reinforcement materials, of metallic or no-metallic nature, can be obtained for precise quality control measures. The goal here was therefore to check whether the intended/expected concrete cover thickness was maintained along the Z-axis of the scanned CRC beams. The concrete cover thickness was measured according to the specifications of Eurocode 2 [31], that is by calculating the distance between the surface of the reinforcement and the nearest concrete surface.

The cover thickness along the Z-axis was computed for the outermost longitudinal warp rovings located in the tension zone of sample B (points 1 and 2 depicted in Figure 6a). Obtained results are shown in Figure 6b. It can be seen that the carbon reinforcement was clearly not in-plane and aligned with the expected concrete cover thickness, which should have been constant along the depth of the sample and equal to 5 mm. The results demonstrate that the carbon grid is slightly tilted and a continuous difference of approximately 2 mm of concrete cover thickness can be observed between points 1 and 2. Also, at depth levels between 0 and 100 mm, concrete cover values higher than 7 mm were registered, which is 40% higher than expected. It is also noteworthy to mention that the results were able to capture with accuracy the localized cover thickness decrease due to notch that was deliberately part of the specimen geometry. This can be observed at depth level equal to circa 180 mm, where a clear dip is shown in the graph.

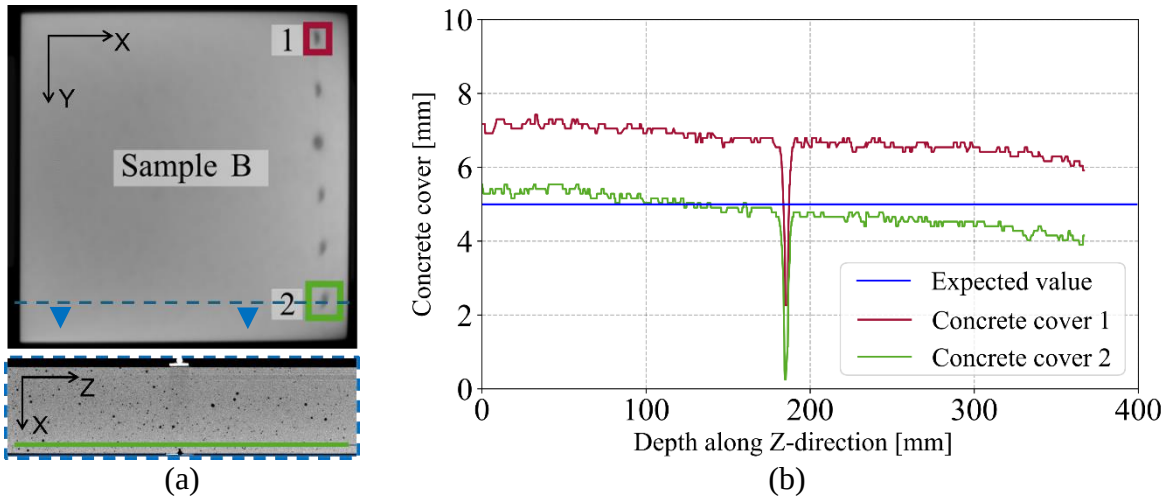


**Figure 6**: Concrete cover thickness for sample B along Z-direction (load step 0): (a) Indication of position 1 and 2 on cross-section and X-Y and X-Z planes; (b) concrete cover thickness along Z-direction

The correct position of the reinforcement elements within a concrete cross-section is of utmost importance for structural concrete members. This is particularly the case for CRC members, since geometries are very thin and filigree, which requires low tolerances. Undesirable shifts of the reinforcement location can lead to important effects on the load-bearing capacity of the overall structure. In the case of structural design processes conducted with recourse to finite element modelling, this type of CT results is able to provide relevant insight on the real position of the reinforcement. The modelling process can, in light of this, be revisited and lead to an improved numerical model. This improved model, with incorporation of found quality defects, can be compared to the original/theoretical model to evaluate possible impacts on structural performance.

## 5 CONCLUSIONS

- This research presents preliminary tests conducted as part of the development process of the tomography portal *Gulliver*, an XXL-CT device being built at the University of Kaiserslautern-Landau. In situ computed tomography tests were in focus, applied to carbon reinforced concrete samples with cross-section 80 × 160 mm$^2$. The results show the potential of using this testing method, which provides detailed 4D data of the whole concrete specimens (3D images over time).
- A collection of CT data intended for direct comparison with numerical models in the meso- to macroscopic scale was generated with recourse to DVC. Results show that DVC can be used to compute displacement fields, to identify crack formation and to measure the corresponding crack width.
- The accuracy of the generated CT data show also relevant potential as quality control tools for concrete structures. In this context, inspections of the manufacturing quality of the scanned CRC samples were carried out by checking if the carbon reinforcement was installed in the correct position.
- This study also showed that the use of high energy during CT scans comes at a cost, as

it tends to introduce significant noise into the reconstructed images. This results in a loss of detailed information in the CT images. However, future research to be conducted in *Gulliver* with this level of employed energy and will involve much larger concrete samples, which will expectedly lead to better texture of the CT data.

## ACKNOWLEDGMENTS

This research work is funded by the German Research Foundation (DFG, Deutsche Forschungsgemeinschaft) – CRC/TRR 280 (project ID 417002380). The authors would like to thank the funding authority for their financial support and the staff of the Civil Engineering Department of RPTU Kaiserslautern-Landau, TU Dresden and Fraunhofer EZRT institute in Fürth for their support extended during the experimental works carried out in the laboratory.

## REFERENCES

[1] Gagg, C. R., "Cement and concrete as an engineering material: An historic appraisal and case study analysis," Engineering Failure Analysis **40**, 114–140 (2014).

[2] Curbach, M., J. Hegger, J. Bielak, C. Schmidt, S. Bosbach, S. Scheerer, M. Claßen, J.-W. Simon, H.-G. Maas, A. Vollpracht, A. Koch, L. Hahn, M. Butler, B. Beckmann, V. Adam, C. Cherif, R. Chudoba, T. Gries, E. Günther, M. Kaliske, S. Klinkel, S. Löhnert, T. Lautenschläger, T. Matschei, V. Mechtcherine, W. E. Nagel, C. Neinhuis, A. Niemeyer, J. R. Noennig, M. Raupach, S. Reese, C. Scheffler, F. Schladitz, M. Traverso, and S. Marx, "New perspectives on carbon reinforced concrete structures—Why new composites need new design strategies," Civil Engineering Design **5**, 67–94 (2024).

[3] Sidiq, A., R. J. Gravina, S. Setunge, and F. Giustozzi, "High-efficiency techniques and micro-structural parameters to evaluate concrete self-healing using X-ray tomography and Mercury Intrusion Porosimetry: A review," Construction and Building Materials **252**, 119030 (2020).

[4] Suleiman, A. R., L. V. Zhang, and M. L. Nehdi, "Quantifying Crack Self-Healing in Concrete with Superabsorbent Polymers under Varying Temperature and Relative Humidity," Sustainability **13**, 13999 (2021).

[5] Skarżyński, Ł., and J. Suchorzewski, "Mechanical and fracture properties of concrete reinforced with recycled and industrial steel fibers using Digital Image Correlation technique and X-ray micro computed tomography," Construction and Building Materials **183**, 283–299 (2018).

[6] Brisard, S., M. Serdar, and P. J. Monteiro, "Multiscale X-ray tomography of cementitious materials: A review," Cement and Concrete Research **128**, 105824 (2020).

[7] Vicente, M. A., D. C. González, and J. Mínguez, "Recent advances in the use of computed tomography in concrete technology and other engineering fields," Micron (Oxford, England : 1993) **118**, 22–34 (2019).

[8] Du Plessis, A., and W. P. Boshoff, "A review of X-ray computed tomography of concrete and asphalt construction materials," Construction and Building Materials **199**, 637–651 (2019).

[9] Grzesiak, S., T. Barisin, K. Schladitz, and M. Pahn, "Analysis of the bond behavior of a GFRP rebar in concrete by in-situ 3D imaging test," Materials and Structures **56**, 163 (2023).
[10] Li, N., Y. Zhao, Y. Xing, X. He, and H. Li, "Meso-damage analysis of concrete based on X-ray CT in-situ compression and using deep learning method," Case Studies in Construction Materials **18**, e02118 (2023).
[11] Nguyen, T., A. Ghazlan, A. Kashani, S. Bordas, and T. Ngo, "3D meso-scale modelling of foamed concrete based on X-ray Computed Tomography," Construction and Building Materials **188**, 583–598 (2018).
[12] Stamati, O., E. Roubin, E. Andò, and Y. Malecot, "Tensile failure of micro-concrete: from mechanical tests to FE meso-model with the help of X-ray tomography," Meccanica **54**, 707–722 (2019).
[13] Skarżyński, Ł., and J. Tejchman, "Experimental Investigations of Fracture Process in Concrete by Means of X-ray Micro-computed Tomography," Strain **52**, 26–45 (2016).
[14] Koudelka, P., T. Fila, V. Rada, P. Zlamal, J. Sleichrt, M. Vopalensky, I. Kumpova, P. Benes, D. Vavrik, L. Vavro, M. Vavro, M. Drdacky, and D. Kytyr, "In-situ X-ray Differential Micro-tomography for Investigation of Water-weakening in Quasi-brittle Materials Subjected to Four-point Bending," Materials (Basel, Switzerland) **13** (2020).
[15] Zhang, X., Z. Yang, M. Pang, Y. Yao, Q. M. Li, and T. J. Marrow, "Ex-situ micro X-ray computed tomography tests and image-based simulation of UHPFRC beams under bending," Cement and Concrete Composites **123**, 104216 (2021).
[16] Khormani, M., V. R. Kalat Jaari, I. Aghayan, S. H. Ghaderi, and A. Ahmadyfard, "Compressive strength determination of concrete specimens using X-ray computed tomography and finite element method," Construction and Building Materials **256**, 119427 (2020).
[17] Auenhammer, R. M., J. Kim, C. Oddy, L. P. Mikkelsen, F. Marone, M. Stampanoni, and L. E. Asp, "X-ray scattering tensor tomography based finite element modelling of heterogeneous materials," npj Comput Mater **10** (2024).
[18] Huang, Y., F. Guo, H. Zhang, and Z.-J. Yang, "An efficient computational framework for generating realistic 3D mesoscale concrete models using micro X-ray computed tomography images and dynamic physics engine," Cement and Concrete Composites **126**, 104347 (2022).
[19] Yang, Z.-J., B.-B. Li, and J.-Y. Wu, "X-ray computed tomography images based phase-field modeling of mesoscopic failure in concrete," Engineering Fracture Mechanics **208**, 151–170 (2019).
[20] Rodrigues, E. A., O. L. Manzoli, and L. A. Bitencourt, "3D concurrent multiscale model for crack propagation in concrete," Computer Methods in Applied Mechanics and Engineering **361**, 112813 (2020).
[21] Homel, M. A., J. Iyer, S. J. Semnani, and E. B. Herbold, "Mesoscale model and X-ray computed micro-tomographic imaging of damage progression in ultra-high-performance concrete," Cement and Concrete Research **157**, 106799 (2022).
[22] Beckmann, B., J. Bielak, S. Bosbach, S. Scheerer, C. Schmidt, J. Hegger, and M. Curbach, "Collaborative research on carbon reinforced concrete structures in the CRC / TRR 280 project," Civil Engineering Design **3**, 99–109 (2021).

[23] Giese, J., M. Herbers, F. Liebold, F. Wagner, S. Grzesiak, C. de Sousa, M. Pahn, H.-G. Maas, S. Marx, M. Curbach, and B. Beckmann, "Investigation of the Crack Behavior of CRC Using 4D Computed Tomography, Photogrammetry, and Fiber Optic Sensing," Buildings **13**, 2595 (2023).

[24] Liebold, F., F. Wagner, J. Giese, S. Grzesiak, C. de Sousa, B. Beckmann, M. Pahn, S. Marx, M. Curbach, and H.-G. Maas, "Damage Analysis and Quality Control of Carbon-Reinforced Concrete Beams Based on In Situ Computed Tomography Tests," Buildings **13**, 2669 (2023).

[25] Tietze, M., S. Kirmse, A. Kahnt, F. Schladitz, and M. Curbach, "The ecological and economic advantages of carbon reinforced concrete—Using the C 3 result house CUBE especially the BOX value chain as an example," Civil Engineering Design **4**, 79–88 (2022).

[26] Giese, J., H. Spartali, B. Beckmann, F. Schladitz, and R. Chudoba, "Experimental Investigation on the Buckling Behavior of Slender TRC Structures," in: A. Ilki, D. Çavunt, and Y. S. Çavunt, eds., Building for the Future: Durable, Sustainable, Resilient (Springer Nature Switzerland, Cham, 2023), 1398–1407.

[27] Bay, B. K., T. S. Smith, D. P. Fyhrie, and M. Saad, "Digital volume correlation: Three-dimensional strain mapping using X-ray tomography," Experimental Mechanics **39**, 217–226 (1999).

[28] Geers, M., R. de Borst, and W. Brekelmans, "Computing strain fields from discrete displacement fields in 2D-solids," International Journal of Solids and Structures **33**, 4293–4307 (1996).

[29] Liebold, F., and H.-G. Maas, "Computational Optimization of the 3D Least-Squares Matching Algorithm by Direct Calculation of Normal Equations," Tomography (Ann Arbor, Mich.) **8**, 760–777 (2022).

[30] Liebold, F., and H.-G. Maas, "3D-Deformationsanalyse und Rissdetektion in multitemporalen Voxeldaten von Röntgentomographen," in Proceedings of Dreiländertagung der DGPF, OVG, SGPF Photogrammetrie-Fernerkundung-Geoinformation-2022, Dresden, Germany, 5-6 October 2022, **30**, 105–116 (2022).

[31] EN 1992-1-1 Eurocode 2: Design of concrete structures - Part 1-1: General ruels and rules for buildingsCEN, en1992 (2005).